ETH *zürich*

Spin–Orbit Coupling and Potential Energy Functions of Ar$_2$# and Kr$_2$# by High-Resolution Photoelectron Spectroscopy and ab Initio Quantum Chemistry

Journal Article

Author(s):
Mastalerz, Remigius; Zehnder, Oliver; Reiher, Markus; Merkt, Frédéric

Spin-orbit coupling and potential energy functions of Ar_2^+ and Kr_2^+ by high-resolution photoelectron spectroscopy and *ab initio* quantum chemistry

R. Mastalerz, O. Zehnder, M. Reiher,[*] and F. Merkt[†]

Laboratorium für Physikalische Chemie,

ETH Zurich, 8093 Zurich, Switzerland

(Dated: March 28, 2012)

Abstract

The dependence of the spin-orbit-coupling constant of the six low-lying electronic states of Ar_2^+ and Kr_2^+ on the internuclear distance R has been calculated ab initio. The spin-orbit-coupling constant varies by about 10% over the range of internuclear distances relevant for the interpretation of the high-resolution photoelectron spectra of Ar_2 and Kr_2 and can be accurately represented by a Morse-type function for the states of *ungerade* electronic symmetry and by an exponentially decreasing function for the states of *gerade* symmetry. The spin-orbit-coupling constant is larger than the asymptotic value (at $R \to \infty$) for the *gerade* states and smaller for the *ungerade* states. The calculated R-dependent spin-orbit-coupling constants were used to derive a new set of potential energy functions for the low-lying electronic states of Ar_2^+ and Kr_2^+ and to quantify the errors resulting from the widely used approach consisting of approximating the spin-orbit-coupling constant by its asymptotic value. The effects of the R dependence on the potential energy functions of the six low-lying electronic states of the homonuclear rare gas dimer ions are found to be very small for Ar_2^+ (and by inference also for Ne_2^+), but significant for Kr_2^+. The shifts arising in calculations of the potential energy functions from a neglect of the R dependence of the spin-orbit-coupling constant are the result of the interplay between the differences between the binding energies of the relevant $^2\Pi$ and $^2\Sigma^+$ states, the magnitude of the spin-orbit-coupling constant, and the magnitude and sign of the deviations between the R-dependent spin-orbit-coupling constant and its asymptotic value at large internuclear distances.

PACS numbers:

---

[*]Electronic address: `markus.reiher@phys.chem.ethz.ch`

[†]Electronic address: `merkt@phys.chem.ethz.ch`

I. INTRODUCTION

The singly charged homonuclear rare-gas dimer ions Rg_2^+ (Rg = Ne, Ar, Kr, and Xe) possess six low-lying electronic states, three of *gerade (g)* and three of *ungerade (u)* electronic symmetry. At short internuclear distances, Hund's angular momentum coupling cases (a) and (b) provide an adequate description of these states, which are labeled A $^2\Sigma_u^+$, B $^2\Pi_{\Omega,g}$, C $^2\Pi_{\Omega,u}$, and D $^2\Sigma_g^+$ ($\Omega = 1/2$ and $3/2$) in the notation used by Mulliken [1]. These states result from the removal of an electron out of one of the outer-valence-shell molecular orbitals $p\sigma_u$, $p\pi_g$, $p\pi_u$ and $p\sigma_g$ that are formed by linear combination of the atomic valence np orbitals ($n = 2$, 3, 4, and 5 for Ne, Ar, Kr, and Xe, respectively). In Hund's case (c) angular momentum coupling scheme, which is appropriate at larger internuclear distances, these states are denoted I(1/2u), I(3/2g), I(3/2u), I(1/2g), II(1/2u), and II(1/2g), where the half-integer number represents the quantum number Ω associated with the projection of the total (spin and orbital) electronic angular momentum onto the internuclear axis, and I and II designate states correlating adiabatically to the $Rg(^1S_0)$ + Rg^+ ($^2P_{3/2}$) and $Rg(^1S_0)$ + Rg^+ ($^2P_{1/2}$) dissociation limits, respectively. Whereas the $\Omega = 3/2$ states have pure Π electronic character, the $\Omega = 1/2$ states have mixed Σ and Π character. The degree of mixing increases with increasing internuclear separation because, at large separation, the spin-orbit interaction becomes stronger than the interatomic interactions and decouples the electronic orbital motion from the internuclear axis.

The quantitative description of these low-lying electronic states in terms of potential energy functions is of practical importance for the characterization of the physical and chemical processes (e.g., charge-exchange [2] and scattering [3] processes) taking place in rare-gas plasmas, such as those arising in excimer lasers [4, 5], rare-gas lamps [6], rare-gas ion lasers [7] and electric space-propulsion thrusters. The potential energy functions of the low-lying electronic states of rare-gas dimer ions are also needed to understand the photoionization dynamics of the neutral rare-gas dimers (see, e.g., [8, 9]), to model the electronically excited (Rydberg) states of Rg_2 [10] and the structure and fragmentation dynamics of larger rare-gas cluster ions [11–13].

In the past decades, a considerable body of information on the low-lying electronic states of Rg_2^+ has been obtained from electronic structure calculations (see, in particular, Refs. [14–30]), from experiments, primarily the photoelectron, photoionization and electron impact ionization spectroscopy [31–53] (including measurements of photofragment kinetic energy distributions [8, 9, 54]), and from a combination of experiment and theory

[55, 56].

Until recently, almost all derivations of the potential energy functions of the six low-lying electronic states of Rg_2^+, be it from *ab-initio* calculations or from experimental data, have relied on a potential model introduced by Cohen and Schneider [57] and characterized by two separate spin-orbit-interaction matrices of the form presented in Table I, one for the three g and one for the three u states. This potential model relies on several assumptions and approximations (see Ref. [58] for a detailed discussion), the most important of which is the assumption that the spin-orbit-coupling constant a does not depend on the internuclear separation and equals $a_{Rg^+} = 2A_{Rg^+}/3$, where A_{Rg^+} represents the separation between the $^2P_{1/2}$ and the $^2P_{3/2}$ spin-orbit components of the ground state of Rg^+. The sign of the spin-orbit-coupling constant a_{Rg^+} of Rg^+ is negative so that, strictly, $2A_{Rg^+}/3 = -a_{Rg^+}$. The form of the spin-orbit-coupling matrix given in Table I assumes a positive value of $a(R)$, which must therefore be interpreted as the absolute value of the spin-orbit-coupling constant. We adopt this convention here to be consistent with earlier work on the potential energy functions of the rare-gas dimer ions [15, 24, 28].

In the case of Xe_2^+, we have recently calculated the R dependence of a and established that a varies by about 10 % over the range of internuclear separation for which experimental observations are available [56]. Beyond $R = 2$ Å, the calculated spin-orbit-coupling functions $a_{g,u}(R)$ for the u and g states could be represented accurately by simple analytical functions, a Morse-type function for the u states and an exponentially decaying function for the g states (see Eqs. (5) and (6) below). The calculated functions $a(R)$ were used to determine a new set of potential energy functions for the six low-lying electronic states of Xe_2^+ in a least-squares fit to high-resolution photoelectron spectroscopic data. The calculation enabled us to quantify the effects of the R dependence of the spin-orbit-coupling constant and led to the conclusion that it needs to be taken into account when deriving potential energy functions using Table I if an absolute accuracy better than 100 cm^{-1} is desired.

We present here an extension of these calculations to the low-lying electronic states of Ar_2^+ and Kr_2^+, two other homonuclear rare-gas dimer cations for which a significant spin-orbit interaction can be expected from the spin-orbit splitting A_{Rg^+} of the ^2P ground state of the atomic ion ($A_{Ar^+} = 1431.5831$ cm^{-1} [59] and $A_{Kr^+} = 5370.294$ cm^{-1} [60]). This work was carried out with the objectives of (i) determining the R dependence of the spin-orbit-coupling constants of the low electronic states of Ar_2^+ and Kr_2^+, (ii) finding out whether the R dependence of the spin-orbit-coupling constant can be described by

3

analytical functions of the same type as in the case of Xe_2^+, (iii) quantifying possible effects of this R dependence on the potential energy functions, and (iv) deriving an improved set of potential energy functions for Ar_2^+ and Kr_2^+ using the calculated spin-orbit-coupling constants in a least-squares fit to available spectroscopic data.

The structure of the article is as follows: After a presentation of the model employed to determine the potential energy functions of the six low-lying electronic states in Section II, the computational methods used to calculate the R-dependent spin-orbit-coupling constant are recapitulated in Section III. The experimental data used to derive the potential energy functions of Ar_2^+ and Kr_2^+ are then summarized in Section IV. The results of the least-squares fit are presented in Sections V where they are compared with the experimental data.

II. POTENTIAL MODEL

The method used to determine the potential energy functions of the six low-lying electronic states of Ar_2^+ and Kr_2^+ relies on the treatment of the spin-orbit interaction by means of the Hamiltonian matrix given in Table I. The electronic energies of these states correspond to the eigenvalues of the matrix and are determined as functions of the internuclear distance R. The method is semi-empirical in nature: It relies on the determination of the R-dependent spin-orbit-coupling constants $a(R)$ by computational methods as described in Section III and on model analytic functions for the potential energy functions V_Σ and V_Π, the parameters of which are determined in least-squares fits to experimental data. The treatment of the spin-orbit interaction corresponds to that introduced by Cohen and Schneider [57], but is improved by the use of R-dependent spin-orbit-coupling functions.

Because the spin-orbit operator only couples states of the same g/u symmetry, two distinct 3×3 matrices are set up, one for the g states, the other for the u states. The spin-orbit interaction matrices are expressed in the basis set adequate for the short-range part of the potentials in which the quantum numbers Λ, Σ, and $\Omega = \Lambda + \Sigma$ corresponding to, respectively, the projection of the total orbital, total electron spin, and total electronic angular momenta onto the internuclear axis are good quantum numbers. Consequently, the electronic potential energies of the $^2\Sigma_{1/2}^+$, $^2\Pi_{1/2}$ and $^2\Pi_{3/2}$ states appear as diagonal elements in the matrix displayed in Table I. The spin-orbit coupling operator is not only described by diagonal (first-order) contributions of $\pm a(R)/2$ which induce a splitting of

4

the $^2\Pi$ state into the two components $^2\Pi_{1/2}$ and $^2\Pi_{3/2}$, but also by off-diagonal (second-order) elements $-a(R)/\sqrt{2}$ which couple states of the same value of Ω, namely the $^2\Sigma^+_{1/2}$ and $^2\Pi_{1/2}$ states [57, 58].

The potential energy functions of the $^2\Sigma^+$ and $^2\Pi$ states under neglect of the spin-orbit interaction are expressed as [49]

$$V_\Lambda(R) = A_\Lambda \mathrm{e}^{-b_\Lambda R} - B_\Lambda\, \mathrm{e}^{-b_\Lambda R/\beta_\Lambda} - \sum_{n=2}^{3} f_{2n}(R, b_\Lambda)\frac{C_{2n,\Lambda}}{R^{2n}} + V_{\mathrm{diss}} \qquad (1)$$

with $\Lambda = \Sigma,\, \Pi$. The first, second, and third terms on the right-hand side of Eq. (1) describe the repulsive interaction at short range, the chemical bonding at intermediate internuclear distances, and the dominant members of the Tang–Toennies long-range interaction series [61], respectively. V_{diss} is a constant used to relate the potential energies to the energy of the $\mathrm{X}\,0^+_\mathrm{g}$ ($v'' = 0$) ground neutral state and is defined as

$$V_{\mathrm{diss}} = D_0(\mathrm{Rg}_2,\, \mathrm{X}\,0^+_g) + E_\mathrm{i}(\mathrm{Rg},\, ^2\mathrm{P}_{3/2} \leftarrow^1 \mathrm{S}_0)/hc + \frac{a_{\mathrm{Rg}^+}}{2}, \qquad (2)$$

where $D_0(\mathrm{Rg}_2,\, \mathrm{X}\,0^+_g)$ represents the dissociation energy of the ground state neutral rare-gas dimer, $E_\mathrm{i}(\mathrm{Rg},\, ^2\mathrm{P}_{3/2} \leftarrow^1 \mathrm{S}_0)$ the first ionization energy of the neutral rare gas atom, and $a_{\mathrm{Rg}^+} = 2A_{\mathrm{Rg}^+}/3$.

After determining the potential energy functions $V_j(R)$ of the three u and the three g states as eigenvalues of the interaction matrix presented in Table I for a given set of parameters in Eq. (1), the calculated positions of the vibrational levels of the electronic state j are obtained by numerically solving the one-dimensional Schrödinger equation

$$\left[-\frac{\hbar^2}{2\mu_i}\frac{\mathrm{d}^2}{\mathrm{d}R^2} + hc\, V_j(R)\right]\psi_{ijv}(R) = E_{ijv}\psi_{ijv}(R) \qquad (3)$$

corresponding to the vibrational motion of the isotopomer with reduced mass μ_i in the potential $V_j(R)$ following the procedure described in Refs. [40, 49]. In Eq. (3) the indices i and v designate the isotopomer and the vibrational quantum number of the ion, respectively.

The optimal set of parameters determining the functions $V_{\Sigma_\mathrm{u}}(R)$, $V_{\Pi_\mathrm{u}}(R)$, $V_{\Sigma_\mathrm{g}}(R)$ and $V_{\Pi_\mathrm{g}}(R)$ are derived by minimizing the deviations between calculated and experimental level positions in a least-squares-fit procedure. The majority of the potential parameters in Eq. (1) are known with sufficient accuracy from experiment or theory that they do not need to be optimized, as will be discussed further in Section V.

III.   COMPUTATIONAL DETAILS

The computational methodology used to obtain the spin-orbit-coupling constant of the lowest-lying Σ and Π states of gerade and ungerade symmetry in Ar_2^+ and Kr_2^+ has already been applied to Xe_2^+ as described in Ref. [56]. Consequently, only aspects specific to Ar_2^+ and Kr_2^+ are summarized here, and we refer to Ref. [56] for additional information. The spin-orbit coupling constant was obtained from *ab initio* data by exploiting the block-diagonal form of the spin-orbit interaction matrix presented in Table I, which allows a calculation of $a(R)$ at a specific internuclear distance R from

$$a(R) = 2\left(E_{el}^{\Pi}(R) - E_{el}^{\Pi_{3/2}}(R) \right), \tag{4}$$

where $E_{el}^{\Pi}(R)$ correspond to the electronic energies of the $^2\Pi$ states without consideration of the spin-orbit interaction and $E_{el}^{\Pi_{3/2}}(R)$ to the energies of the $^2\Pi_{3/2}$ electronic states which are equivalent to the I($3/2u$ or g) states within the approximations implied by Table I.

Davidson-corrected multi-reference configuration interaction all-electron calculations with singles and doubles excitations (MRCISD+Q) were performed employing the scalar-relativistic second-order Douglas–Kroll–Hess (DKH) Hamiltonian [62] in combination with the ANO-RCC basis sets of Roos *et al.* [63]. The basis sets were used in a fully de-contracted form, resulting in the overall sizes of (17s/12p/5d/4f/2g) in the case of Ar and (20s/17p/11d/4f/2g) in the case of Kr. 35 electrons were explicitly correlated in the MRCISD+Q calculations, corresponding to the 1s, 2s, 2p, 3s and 3p shell of Ar and the 3d, 4s and 4p shell of Kr. The spin-orbit interaction was considered as a perturbation and treated in an *a posteriori* procedure.

The energies of the six lowest-lying Hund's-case-(c)-coupled states, in particular the energy $E_{el}^{\pi_{3/2}}$ of the $^2\Pi_{3/2}$ state that is needed to evaluate Eq. (4), were obtained from a state-interaction approach by diagonalizing the matrix representation of the electronic Hamiltonian and the spin-orbit Hamiltonian in the basis of the eigenfunctions of the electronic Hamiltonian. The spin-orbit matrix was constructed in a truncated basis set ((17s/12p/5d) for Ar and (20s/17p/11d) for Kr). Its elements were set up from the spin-orbit part of the Breit–Pauli Hamiltonian in the case of internal configurations, whereas an effective mean-field Fock-operator [64] was employed for external configurations. All diagonal elements of the resulting spin-orbit matrix, however, were shifted in energy to correspond to the MRCISD+Q energies obtained with the complete de-contracted basis sets. The MRCI calculations were performed with the MOLPRO2002.6 program suite

[65]. The potential energy curves were determined for internuclear distances ranging from 3.5 to 14.0 a_0 in the case of Kr_2^+ and 2.5 to 10.0 a_0 in the case of Ar_2^+ (a_0 is the Bohr radius).

The R dependences of the spin-orbit coupling constants calculated for Ar_2^+, Kr_2^+ are depicted in Fig.1 where they are compared with the results obtained previously for Xe_2^+ [56] and with the experimental values of the asymptotic spin-orbit-coupling constants a calculated from $a_{Rg^+} = \frac{2}{3} A_{Rg^+}$, where A denotes the energy splitting between the $^2P_{1/2}$ and $^2P_{3/2}$ states of the corresponding rare-gas atomic ion. As already noticed in the case of Xe_2^+, the R-dependent spin-orbit-coupling functions of the g and u states follow a different pattern at short internuclear distances: $a_u(R)$ drops significantly below the asymptotic value whereas $a_g(R)$ becomes significantly larger than $\frac{2}{3} A_{Rg^+}$. In the vicinity of the dissociation limit of Ar_2^+ (i.e., for $R \to \infty$), the theoretical value of a agrees with the experimental value within better than 3 cm^{-1}, which represents a deviation of only 0.3% (see top panel of Fig. 1). In the case of Kr_2^+ (middle panel of Fig. 1), the MRCISD+Q spin-orbit calculations predict the asymptotic value of a to be approximately 100 cm^{-1} (i.e., about 2.8%) less than the experimental value. The deviation between calculated and experimental values of the asymptotic spin-orbit couling constant is largest in the case of Xe_2^+ (bottom panel of Fig. 1), the calculations overestimating it by about 500 cm^{-1} , or almost 7% [56].

The decrease of the accuracy of the calculations of the spin-orbit-coupling functions from Ar_2^+ to Xe_2^+ that is betrayed by the increasing deviation between computed and experimental asymptotic values has two main causes: The first is related to the decreasing quality of the electron-correlation treatment in the MRCISD+Q calculations. In the MRCISD+Q calculation on Ar_2^+, no frozen-core approximation was needed, because all electrons could be explicitly included in the electron-correlation procedure, which resulted in accurate unperturbed wave functions for the subsequent spin-orbit calculation. In contrast, the MRCISD+Q calculations on the heavier dimer ions had to be performed with a predefined frozen core of 36 and 72 (non-correlated) electrons in the case of Kr_2^+ (total number of electrons: 71) and Xe_2^+ (total number of electrons: 107, see Ref. [56]), respectively. The resulting unperturbed wave functions are therefore less accurate than in the case of Ar_2^+. The second cause is the increasing magnitude of the spin-orbit interaction combined with the fact that the interaction is treated as a first-order perturbation in the subsequent state-interaction approach. This combination inevitably results in a loss of accuracy.

7

The derivation of the potential energy functions by the least-squares fit procedure described in Section II requires the matrix elements of Table I to be expressed in analytical form. In the range of internuclear distances relevant to the experimental observations, the spin-orbit-coupling constant a_g and a_u of the *gerade* and *ungerade* states can be almost perfectly described by the expressions

$$a_u(R) = a_{\text{Rg}^+} - a_{u,0} \cdot \left(1 - \left[1 - \exp\left(-a_{u,1} \cdot (R/\text{Å} - a_{u,2}) \right) \right]^2 \right) \tag{5}$$

and

$$a_g(R) = a_{\text{Rg}^+} + a_{g,0} \cdot \exp(-a_{g,1} \cdot (R/\text{Å})^{a_{g,2}}), \tag{6}$$

respectively, in which $a_{\text{Rg}^+} = \frac{2}{3} A_{\text{Rg}^+}$ represents the asymptotic value (Rg=Ar, Kr). Eq. (5) is a Morse-type function and Eq. (6) falls exponentially with increasing R value. In order to derive as accurate spin-orbit-coupling functions as possible from the *ab-initio* calculations, the following two-step procedure was followed: First, the computed constants were scaled linearly so that the asymptotic value exactly matched the experimental value determined by atomic spectroscopy, i.e., $a(R \to \infty) = 2A_{\text{Rg}^+}/3$, with $A_{\text{Rg}^+} = \left[E(\text{Rg}^+,{}^2\text{P}_{1/2}) - E(\text{Rg}^+,{}^2\text{P}_{3/2}) \right]/hc$. Then, the parameters $a_{u,i}$ and $a_{g,i}$ ($i = 0, 1, 2$) were determined from the scaled *ab-initio* data in a least-squares-fit procedure. The optimal parameters $a_{u,i}$ and $a_{g,i}$ ($i = 0, 1, 2$) are listed in Table II where they are compared with the values determined for Xe_2^+ in Ref. [56].

This two-step procedure is illustrated in Figs. 2 and 3 for Ar_2^+ and Kr_2^+, respectively, where the open circles and squares represent the values calculated *ab initio*, the full circles and squares the scaled spin-orbit coupling constants with correct asymptotic value, and the full lines the results of least-squares fits based on Eqs. (5) and (6).

The spin-orbit-coupling functions presented in Table II and Figs. 2 and 3 represent the main results of the computational part of this article. The fact that Eqs. (5) and (6) perfectly describe the shape of the calculated spin-orbit-coupling functions of all three dimer ions makes us confident that these functions are well suited to describe the R dependence of the spin-orbit-coupling constants in these molecules and related molecular systems such as Y_2^- (Y=F, Cl, Br, and I). Because of the semi-empirical nature of the scaling procedure, we further expect these functions to describe the R dependence of a_g and a_u sufficiently accurately that they can be held fixed when deriving the potential energy functions from experimental data using the matrix presented in Table I.

IV. EXPERIMENTAL DATA

The experimental data used to derive the potential energy functions of the six low-lying electronic states of Ar_2^+ and Kr_2^+ stem from studies of the pulsed-field-ionization zero-kinetic-energy (PFI-ZEKE) photoelectron spectra of Ar_2 [39, 40, 45, 46] and Kr_2 [43, 44, 52]. Details concerning the measurement procedure, the assignment of the spectra, and the estimation of the experimental uncertainties in the spectral positions have been given in the original publications.

In the case of Ar_2^+, the data set consists of the positions of the $I(1/2u, v^+ = 3, 5\text{-}10, 12\text{-}50)$, $I(3/2u, v^+ = 0)$ and $II(1/2u, v^+ = 0-2)$ levels of $^{40}Ar_2^+$ and the $I(1/2u, v^+ = 20, 21)$ levels of $^{36}Ar_2^+$ measured by single-photon PFI-ZEKE photoelectron spectroscopy [39, 40], and of the $I(1/2u, v^+ = 35\text{-}50)$, $I(3/2g, v^+ = 0-10)$, $I(3/2u, v^+ = 0-2)$, $I(1/2g, v^+ = 1-5)$ and $II(1/2u, v^+ = 0-2)$ levels of $^{40}Ar_2^+$ and the $I(1/2u, v^+ = 38\text{-}46)$, $I(3/2g, v^+ = 0-7)$, $I(3/2u, v^+ = 0-2)$, $I(1/2g, v^+ = 3, 4)$ and $II(1/2u, v^+ = 0-2)$ levels of $^{36}Ar_2^+$, all measured with rotational resolution by $(1+1')$ resonance-enhanced two-photon excitation via selected rovibrational levels of the 0_u^+ level of Ar_2 located below the Ar $4s[1/2]_1 + Ar\ ^1S_0$ dissociation threshold [45, 46]. These data were summarized in Ref. [49] and employed to extract potential energy functions of the six low-lying electronic states of Ar_2^+ in a global fit based on the assumption of an R-independent spin-orbit-coupling constant.

In the case of Kr_2^+, the data set consists of the positions of the $I(1/2u, v^+ = 0, 1, 5, 6, 15\text{-}18, 20, 22, 24\text{-}29, 32, 33, 35\text{-}53)$, $I(3/2u, v^+ = 0\text{-}2)$ and $II(1/2u, v^+ = 0-8)$ levels of several isotopomers of Kr_2^+ determined by single-photon PFI-ZEKE photoelectron spectroscopy [43], and the positions of the $I(1/2u, v^+ = 55\text{-}60, 62\text{-}67, 69, 73, 74)$, $I(3/2u, v^+ = 0\text{-}10)$ and $II(1/2u, v^+ = 0-8)$ levels of $^{84}Kr_2^+$ and of the $I(1/2u, v^+ = 56\text{-}60)$, $I(3/2u, v^+ = 0\text{-}6)$ and $II(1/2u, v^+ = 3-9)$ levels of $^{86}Kr^{84}Kr^+$ measured by PFI-ZEKE photoelectron spectroscopy following $(2+1')$ resonant three-photon excitation via the 0_g^+ Rydberg state of Kr_2 located below the Kr $5p[1/2]_0 + Kr\ ^1S_0$ dissociation threshold [44, 52]. Because of the small rotational constants of Kr_2 and Kr_2^+, the rotational structure of the PFI-ZEKE photoelectron spectra could not be resolved. The positions of the ionic vibrational levels with respect to that of the neutral ground state were therefore assumed to correspond to the maximum of the smooth intensity distributions resulting from the unresolved rotational structure of the relevant bands. Possible errors induced by this procedure were included in the experimental uncertainties. The observed spec-

9

tral positions $\tilde{\nu}_{obs}$ and their experimental uncertainties are summarized in the Appendix in Tables VII-XI for Ar_2^+ and Tables XII-XIV for Kr_2^+, where they are compared with the positions calculated from the potential energy functions determined in this work, as explained in the next section.

The experimental data set just described contains information on all low-lying electronic states of Ar_2^+ and Kr_2^+ except the II($1/2g$) state of Ar_2^+ and the I($1/2g$) and II($1/2g$) states of Kr_2^+. These three states are very weakly bound and attempts at observing their (ro)vibrational energy level structure have remained unsuccessful so far. Because the spin-orbit-coupling matrix (Table I) necessitates the knowledge of at least two of the three states of g or u symmetry, the experimental data on Ar_2^+ are sufficient, in combination with the calculated R-dependent spin-orbit-coupling matrix, to extract the potential energy functions of all six low-lying states and to estimate the positions of the so far unobserved vibrational levels of the II ($1/2g$) state. The potential energy functions of the g states of Kr_2^+, however, cannot be determined from the experimental data set.

V. THE POTENTIAL ENERGY FUNCTIONS OF THE LOW-LYING ELECTRONIC STATES OF AR_2^+ AND KR_2^+

One of the major advantages of the procedure described in Section II to determine the potential energy functions of the low-lying electronic states of the rare-gas-dimer ions from experimental data, next to the fact that it includes the R dependence of the spin-orbit-coupling constant, is the small number of potential parameters that need to be optimized. The three coupled potential functions can be obtained by adjusting only eight parameters (the coefficients A_Λ, B_Λ, b_Λ and β_Λ for $\Lambda = \Sigma$ and Π) for the u states, and seven for the g states. Indeed, the second term in Eq. (1), which describes the chemical bond, can be neglected for the $^2\Sigma_g^+$ state ($B_{\Sigma_g} = 0$) because it is only very weakly bound. Rather than optimizing the parameters A_Λ and B_Λ, it turned out to be advantageous to optimize the equilibrium distance R_e and the dissociation energy D_e with which A_Λ and B_Λ can be calculated using the conditions by (see Appendix A of Ref. [49])

$$\left. \frac{dV_\Lambda(R)}{dR} \right|_{R=R_{e,\Lambda}} = 0 \tag{7}$$

and

$$V_\Lambda(R_{e,\Lambda}) = V_{\text{diss}} - D_{e,\Lambda}. \tag{8}$$

The coefficients $C_{2n,\Lambda}$ of the Tang–Toennies long-range expansion series [61] were taken

10

from Refs. [52, 66, 67]. The values of $V_{\text{diss}}(^{40}\text{Ar}_2) = 127671.48\,\text{cm}^{-1}$, $V_{\text{diss}}(^{36}\text{Ar}_2) = 127670.686\,\text{cm}^{-1}$, and $V_{\text{diss}}(\text{Kr}_2) = 118411.5\,\text{cm}^{-1}$ were obtained from the literature values $a_{\text{Ar}^+} = \frac{2}{3}A_{\text{Ar}^+} = 954.3887\,\text{cm}^{-1}$ [59], $a_{\text{Kr}^+} = \frac{2}{3}A_{\text{Kr}^+} = 3580.196\,\text{cm}^{-1}$ [60], $E_{\text{i}}(\text{Ar}, {}^2\text{P}_{3/2})/hc = 127109.842\,\text{cm}^{-1}$ [68], $E_{\text{i}}(\text{Kr}, {}^2\text{P}_{3/2})/hc = 112914.434\,\text{cm}^{-1}$ [69], $D_0(^{40}\text{Ar}_2,\, \text{X}\,0_g^+) = 84.44\,\text{cm}^{-1}$, $D_0(^{36}\text{Ar}_2,\, \text{X}\,0_g^+) = 83.65\,\text{cm}^{-1}$ and $D_0(^{84}\text{Kr} -^{86}\text{Kr},\, 0_g^+) \approx D_0(^{84}\text{Kr}_2,\, \text{X}\,0_g^+) = 126.8\,\text{cm}^{-1}$ [70, 71]. The dissociation energies of the neutral Ar_2 dimers were calculated by solving the radial Schrödinger equation for the ground electronic state with the interaction potential reported by Tang and Toennies [61] using the same procedure as described in Ref. [72] for Ne_2.

Weighted least-squares fits of the potential parameters were carried out separately for the u and g states. The quality of the fits was assessed from the normalized root-mean-square deviation (rms value of the fit), which is given by $\sqrt{\chi^2/n}$, where $n = N - P$ represents the number of degrees of freedom, i.e., the difference between the number of experimental data points N and the number of adjustable parameters P, and

$$\chi^2 = \sum_{i=1}^{N} \left(\frac{\tilde{\nu}_i^{obs} - \tilde{\nu}_i^{calc}}{\sigma_i} \right)^2. \tag{9}$$

The value of the experimental uncertainties are listed with the level positions in the tables of the appendix, which also compare the positions of the vibrational levels of Ar_2^+ and Kr_2^+ with those calculated from the potential energy functions.

The results of the least-squares fits for Ar_2^+ and Kr_2^+ are presented in the next two subsections and serve as basis for the discussion of the effects of the R dependence of the spin-orbit-coupling constant on the potential functions and energy levels of Ar_2^+ and Kr_2^+.

A. Ar_2^+

A total of 69 (26) experimental level positions were used in the fit of the u (g) states of Ar_2^+, 52 (16) for $^{40}\text{Ar}_2^+$ and 17 (10) for $^{36}\text{Ar}_2^+$, as described in Section IV (see also Tables VII - XI in the Appendix). The results of the fits are summarized in Table III which contains the numerical values of all parameters needed to compute the potential energy functions of the six low-lying electronic states of Ar_2^+ using Eq. (1) and Table I, including the parameters that were kept constant in the fitting procedure.

The rms value of the fits of the u and g states are both slightly less than 1, which indicates that the potential energy functions describe the experimental data well. Table III also contains the dissociation energy and the equilibrium internuclear distances

of the fictive $^2\Sigma^+$ and $^2\Pi$ states. As expected from earlier work and also from simple considerations based on linear combinations of the atomic p valence orbitals, only the $^2\Sigma_u^+$ state is strongly bound, and the $^2\Sigma_g^+$ state is repulsive at short range.

The equilibrium internuclear separations and dissociation energies of the six low-lying states of Ar_2^+ are given in Table IV where they are compared with the results of selected high-level ab-initio calculations [24, 29] (both relying on the assumption of an R-independent spin-orbit couling constant $a = a_{Ar^+}$).

They are also compared with the values obtained in Ref. [49] which relied on the same experimental data set and the same procedure as the present work, except that the spin-orbit-coupling constant was assumed to be independent of R. The similarity of the results obtained from these two fits suggests that the effects of the R dependence of a are weak. Indeed, inspection of the potential energy functions derived from both fits and displayed in Figs. 4 and 5 only reveals significant deviations at short internuclear distances, where the potential energy functions are not constrained by the experimental observations. However, the comparison does not enable one to precisely quantify the effects of the R dependence on the potential functions because these effects are likely to be compensated by other fit parameters.

To quantify the consequences of approximating the spin-orbit-coupling constant to the atomic value a_{Ar^+}, two sets of calculations were performed relying on the same potential energy functions $V_\Sigma(R)$ and $V_\Pi(R)$, as given in Table III, one using the R-dependent functions $a_{g,u}(R)$ presented in Section III, the other using $a_{g,u} = a_{Ar^+}$. The results of these calculations for the u states are depicted in Fig. 6 which compares the potential energy functions on the left-hand side and shows their difference on the right-hand side. The dashed horizontal lines in the figure indicate the highest vibrational levels observed for each electronic state and enable one to directly see the range of internuclear distances covered by the experimental data, i.e., 2 - 4.5 Å for the I$(1/2u)$ state, 3.5 - 4.5 Å for the I$(3/2u)$ state, and 3.3 - 4.2 Å for the II$(1/2u)$ state.

Fig. 6 shows that the neglect of the R dependence of a has an extremely small effect on the potential energy functions of I$(1/2u)$, the differences being less than 2 cm^{-1} over the entire range of internuclear distances. The differences are larger for the I$(3/2u)$ and II$(1/2u)$ states, particular below 3 Å where they reach values up to 45 cm^{-1}, but they remain very small (less than 5 cm^{-1}) over the range of internuclear separation relevant for the analysis of the photoelectron spectroscopic data. The deviations are of the same magnitude but opposite sign for the I$(3/2u)$ and II$(1/2u)$ states. This behavior indicates

12

that the dominant effect originates from the diagonal (first-order) contribution of the spin-orbit operator in Table I. The value of the spin-orbit-coupling functions $a_u(R)$ is less than a_{Ar^+} so that the splitting between the two components of the Π_u state is slightly reduced. This effect raises (lowers) the potential energy of the I(3/2u) (II(1/2u)) state in the calculations performed with the R-dependent spin-orbit-coupling constant. The very small shift of the I(1/2u) potential energy curves is caused by the off-diagonal (second-order) spin-orbit-coupling matrix elements in Table I and can be explained by the fact that the spin-orbit-coupling constant is much smaller than the difference between the Σ_u^+ and Π_u potential functions in the range of R values where $a_u(R)$ significantly deviates from the asymptotic value a_{Ar^+}. The difference of the binding energies of the Σ_u^+ and Π_u states in the vicinity of the potential minima is indeed more than 10 times larger than the spin-orbit-coupling constant.

Similar conclusions apply to the *gerade* states of Ar_2^+ if one takes into account the different energetic ordering of the Π and Σ states ($^2\Sigma_g^+$ lies above $^2\Pi_g$), the smaller difference in the binding energies of these to states (see Table III), and the fact that $a_g(R)$ is larger than a_{Ar^+} (see Figure 2). Consequently, the I(3/2g) [II(1/2g)] curve calculated with $a_g(R)$ lies below [above] that calculated with a_{Ar^+}. The two $\Omega = 1/2$ states are more strongly mixed, so that the shifts of the I(3/2g) and II(1/2g) states are less symmetric than is the case for the I(3/2u) and II(1/2u) states.

B. Kr_2^+

A total of 91 experimental level positions were used in the fit of the *ungerade* states of Kr_2^+, 72 for $^{84}Kr_2^+$ and 19 for $^{86}Kr^{84}Kr^+$, as described in Section IV (see also Tables XII-XIV in the appendix). The high-resolution photoelectron-spectroscopic data on the *gerade* states are limited to the I(3/2g) state and are insufficient for a global treatment of these states based on the spin-orbit interaction matrix presented in Table I. This subsection thus focuses on the least-squares fit of the *ungerade* states I(1/2u), I(3/2u), and II(1/2u). The same experimental data set was used in the derivation of the potential energy curves of these states under the assumption of an R-independent spin-orbit-coupling constant [52].

The optimal fit parameters are listed in Table V. Only eight of these were varied in the fitting procedure, as explained in Section II, the remaining ones being kept at the literature values indicated in the table. The rms value of the fit was 1.2, about half the

rms value of 2.2 obtained in the analysis based on the assumption of an R-independent spin-orbit-coupling constant [52]. The dissociation energies of the fictive $^2\Sigma_u^+$ and $^2\Pi_u$ states (10922.5 cm^{-1} and 392 cm^{-1}, respectively) are similar to the values found for Ar$_2^+$, as expected.

The potential energy functions of the three low-lying u states of Kr$_2^+$ are displayed in Fig. 7. Their dissociation energies and equilibrium internuclear distances are compared with the results of earlier investigations in Table VI. Comparing the present results with those obtained assuming an R-independent spin-orbit-coupling constant in Ref. [52] leads to the conclusion that the main discrepancy affects the II(1/2u) state for which a systematic trend in the residuals from +7.6 cm^{-1} at $v = 0$ to -5.7 cm^{-1} at $v = 8$ was noted in Ref. [52] (see Table 3 of this reference). The present analysis is free of this trend and yields a dissociation energy of 1099.8 cm^{-1} for the II(1/2u) state, in better agreement with the value of 1099.9 $\pm$2.1 cm^{-1} determined experimentally in Ref. [43]. This observation, combined with the improved rms value, indicates that the consideration of the R dependence of a leads to potential curves of higher accuracy, particularly for the II(1/2u) state.

To quantify the effects of the assumption of an R-independent spin-orbit-coupling constant used in previous work on the low-lying electronic states of Kr$_2^+$, the same procedure was used as described in the previous subsection for Ar$_2^+$. The results are presented in Fig. 8, which displays, on the left-hand side, the two sets of curves calculated with the same potential functions V_Σ and V_Π (with parameters as given in Table V) but using the function $a_u(R)$ determined in Section III in one case (full line), and a_{Kr^+} in the other (dashed lines). The differences between these two set of curves are plotted on the right-hand side of the figure.

The overall trends of the differences are similar to those observed for Ar$_2^+$ in Fig. 6, but the deviations are 4-5 times larger. While in the case of Ar$_2^+$ the deviations of less than 5 cm^{-1} are of the same order of magnitude as the experimental uncertainties, they are larger in the case of Kr$_2^+$, which makes the effects of the R-dependence of a detectable. Over the range of R values for which experimental data are available (indicated by the dashed horizontal lines in Fig. 8), i.e., 2.2-5 Å for the I(1/2u) state, 3.6-5.6 Å for the I(3/2u) state, and 3.4-4.5 Å for the II(1/2u) state, the deviations vary from 5 to 20 cm^{-1} for the I(1/2u) state, 2 to 20 cm^{-1} for the I(3/2u) state, and 5 to 60 cm^{-1} for the II(1/2u) state. The particularly large deviations predicted for the II(1/2u) state nicely explain why the consideration of the R dependence of the spin-orbit-coupling constant is necessary to

satisfactorily account for the experimental data obtained for this state.

The larger effects of the R dependence of the spin-orbit couling constant in Kr_2^+ compared to Ar_2^+ result from three simultaneous effects: (i) The absolute value of the spin-orbit-coupling constant increases from ≈ 950 cm^{-1} in Ar_2^+ to ≈ 3500 cm^{-1} in Kr_2^+ while (ii) the difference in binding energies of the Σ and Π states is roughly the same for both ions (i.e., about 10000 cm^{-1}), and (iii) the absolute value of the deviations between $a(R)$ and a_{Rg^+} are three times larger in Kr_2^+ (up to 300 cm^{-1}) than in Ar (up to 100 cm^{-1}). Effect (iii) directly influences the potential energies of the I(3/2u), and II(1/2u), I(3/2g), and I(I/2g) states via the diagonal (first-order) elements of the spin-orbit-coupling matrix, and the combination of (i) and (ii) leads to a larger mixing of the two $\Omega = 1/2$ states induced by the off-diagonal elements of the spin-orbit-coupling matrix in the case of Kr_2^+ than in the case of Ar_2^+. The mixing of the $\Omega = 1/2$ levels and the effects of the R dependence of the spin-orbit-coupling constant are expected to be even larger on the *gerade* states of Kr_2^+ because the difference in binding energies of the $^2\Pi_g$ and $^2\Sigma_g^+$ states is smaller in the range of internuclear distances where $a_g(R)$ strongly deviates from a_{Kr^+}. The R dependence of a_g is thus expected to result in a destabilization of II(1/2g) state and may be the main reason why this state, and also the II(1/2g) of Xe_2^+, have not been observed yet in high-resolution photoelectron spectroscopic experiments.

VI. CONCLUSIONS

The spin-orbit interaction strongly influences the structural and spectral properties of the homonuclear rare-gas dimer ions (Rg_2^+, Rg=Ne, Ar, Kr, Xe). Until recently, the spin-orbit-coupling constants used in the derivation of the potential energy functions of the six low-lying electronic states of these molecular ions were assumed to be independent of the internuclear separation and equal to their "atomic" value a_{Rg^+}. Together with our previous investigation of the potential energy functions of Xe_2^+, the investigation of the potential energy functions of the low-lying electronic states of Ar_2^+ and Kr_2^+ presented in this article provides a quantification of the R dependence of the spin-orbit constant in these systems and a systematic examination of the consequences associated with its neglect.

The spin-orbit-coupling constant maximally deviates from the atomic value by up to about 10%, and the deviations have opposite signs for the electronic states of *gerade* and *ungerade* symmetry. The R dependences can be accurately represented by analytical

functions, a Morse-type function for the *ungerade* states and an exponentially decaying function for the *gerade* states. The effects of the R dependence on the potential energy functions are almost entirely negligible for Ar_2^+ (and by inference also for Ne_2^+). They manifest themselves as shifts of the potential energy functions and spin-rovibronic energy levels of at most a few cm^{-1} and are expected to only be observable in very high-resolution spectroscopic measurements. In Kr_2^+ and Xe_2^+, the R dependence leads to more pronounced effects and needs to be considered in the analysis of high-resolution photoelectron spectra and in the description of the potential energy functions of the low-lying electronic states.

The increasingly important impact of the R dependence of the spin-orbit-coupling constant on the properties of the *ungerade* states from Ne_2^+ to Xe_2^+ can be explained by the fact that the difference in binding energies between the $^2\Pi_u$ and $^2\Sigma_u^+$ states that are coupled by the spin-orbit interaction slowly decreases, from about 12000 cm^{-1} in Ne_2^+ [29] to about 9000 cm^{-1} in Xe_2^+ [56] whereas the atomic spin-orbit-coupling constant rapidly increases from about 520.282 cm^{-1} in Ne_2^+ [59] to 7024.617 cm^{-1} in Xe_2^+ [73].

The effects of the spin-orbit interaction on the $^2\Sigma_u^+$ state originate from the off-diagonal element of the spin-orbit interaction matrix, which couples it to the upper $^2\Pi_u$ component of the $^2\Pi$ states. Because the $^2\Sigma_u^+$ state lies below the $^2\Pi_u$ state, the interaction shifts the potential energy function of the former state towards lower energies and that of the latter towards higher energies. The R-dependent spin-orbit-coupling constants of the u states are reduced compared to the atomic value, so that assuming the spin-orbit constant to be independent of R leads to an overestimation of the potential energies. The range of internuclear distances where the spin-orbit-coupling constant significantly deviates from the atomic value corresponds closely to the region where the $^2\Sigma_u^+$ state is strongly bound. In this region, the mixing between the $^2\Sigma_u^+$ and the $^2\Pi_{1/2u}$ states is very weak in Ne_2^+ and Ar_2^+, because the spin-orbit constant is too small to induce a significant mixing between these two states. The effect of the R dependence of a_u is thus negligible in these two molecular ions. In Kr_2^+ and Xe_2^+ the spin-orbit-coupling constant is larger, and the level shifts resulting from the R dependence of the spin-orbit-coupling constant (or its neglect) are on the order of about 20 cm^{-1} for the I(1/2u) state of Kr_2^+ (see Fig. 6) and 50 cm^{-1} for the I(1/2u) state of Xe_2^+ (see Fig. 7d of Ref. [56]) and thus easily observable spectroscopically.

The effects of the R dependence of the spin-orbit-coupling constant on the I(3/2u) state originates from the diagonal (first-order) contribution $(-a(R)/2)$ of the Hamiltonian. The

potential energy shifts resulting from the R dependence of the spin-orbit-coupling constant (or its neglect) thus closely track the value $|(a(R) - a_{\mathrm{Rg}^+})|/2$. These shifts are in general much larger than the shifts arising from the off-diagonal coupling.

The effects of the R dependence of the spin-orbit-coupling constant of the $\mathrm{II}(1/2u)$ state are an additive combination of the two effects described above for the $\mathrm{I}(1/2u)$ and $\mathrm{I}(3/2u)$ states. They are thus largest for this state although strongly dominated by the diagonal contribution of the spin-orbit-coupling matrix. Consequently, the potential energy shifts of the $\mathrm{I}(3/2u)$ and $\mathrm{II}(1/2u)$ states resulting from a neglect of the R dependence of the spin-orbit constant are of similar magnitude but of opposite signs (see upper two panels on the right-hand side of Figs. 6 and 8 and of Fig. 7 of Ref. [52]).

The effect of the R dependence of the spin-orbit-coupling constant on the *gerade* electronic states can be described by the same arguments, taking into account the facts that (i) the function $a(R)$ is larger than a_{Rg^+}, (ii) the $^2\Sigma_g^+$ state is less strongly bound than the $^2\Pi_g$ state, and (iii) the diagonal contribution of the spin-orbit component shifts the upper spin-orbit component of the $^2\Pi_g$ state toward the $^2\Sigma_g^+$ state. While the effects of the R dependence of the spin-orbit-coupling constants are still almost negligible in Ne_2^+ and Ar_2^+ for the same reasons as for the *ungerade* states, the shifts resulting from the R dependence (or its neglect) are expected to be of opposite signs, and the shifts arising from the off-diagonal contribution to be more pronounced, than for the *ungerade* states.

The experimental data available on the $\mathrm{I}(1/2g)$ and $\mathrm{II}(1/2g)$ states of Ar_2^+ and Kr_2^+ are still very incomplete as a result of the repulsive nature of these states at short internuclear distances. In future, one may be able to obtain information on the repulsive part of the potential energy functions of these states by imaging techniques, as was recently demonstrated for Xe_2^+ in Ref. [8].

Appendix

The tables presented in this appendix provide a complete list of the positions of the vibrational levels of Ar_2^+ and Kr_2^+ measured experimentally by pulsed-field ionization zero-kinetic-energy photoelectron spectroscopy. The tables also contain the experimental uncertainties used in the least-squares fits and the deviations between experimental positions and those calculated with the new sets of potential energy functions described in this article. Further details specific to the different tables are provided in the respective table captions.

---

[1] Mulliken, R. S. *J. Chem. Phys.* **1970,** *52,* 5170–5180.

[2] Miller, J. S.; Pullins, S. H.; Levandier, D. J.; hui Chiu, Y.; Dressler, R. A. *J. Appl. Phys.* **2002,** *91,* 984–991.

[3] Boyd, I. D.; Dressler, R. A. *J. Appl. Phys.* **2002,** *92,* 1764–1774.

[4] Rhodes, Ch. K., Ed.; *Excimer Lasers;* volume 30 of *Topics in Applied Physics* Springer: Berlin, 2nd ed.; 1984.

[5] Eden, J. G. *IEEE J. Sel. Top. Quantum Electron.* **2000,** *6,* 1051–1060.

[6] Samson, J. A. R.; Ederer, D. L., Eds.; *Vacuum Ultraviolet Spectroscopy;* Academic Press: San Diego, 2000.

[7] Ewing, J. J. *IEEE J. Sel. Top. Quantum Electron.* **2000,** *6,* 1061–1071.

[8] Shubert, V. A.; Pratt, S. T. *J. Chem. Phys.* **2011,** *134,* 044315.

[9] Hopkins, W. S.; Mackenzie, S. R. *J. Chem. Phys.* **2011,** *135,* 081104.

[10] Piticco, L.; Schäfer, M.; Merkt, F. *J. Chem. Phys.* **2012,** submitted.

[11] Kalus, R.; Paidarová, I.; Hrivňák, D.; Paška, P.; Gadéa, F. X. *Chem. Phys.* **2003,** *294,* 141–153.

[12] Kalus, R.; Paidarová, I.; Hrivňák, D.; Gadéa, F. X. *Chem. Phys.* **2004,** *298,* 155–166.

[13] Poterya, V.; Fárník, M.; Buck, U.; Bonhommeau, D.; Halberstadt, N. *Int. J. Mass Spectrom.* **2009,** *280,* 78-84.

[14] Gilbert, T. L.; Wahl, A. C. *J. Chem. Phys.* **1971,** *55,* 5247–5261.

[15] Michels, H. H.; Hobbs, R. H.; Wright, L. A. *J. Chem. Phys.* **1978,** *69,* 5151–5162.

[16] Wadt, W. R.; Cartwright, D. C.; Cohen, J. S. *Appl. Phys. Lett.* **1977,** *31,* 672–674.

[17] Wadt, W. R. *J. Chem. Phys.* **1978,** *68,* 402–414.

[18] Wadt, W. R. *J. Chem. Phys.* **1980,** *73,* 3915–3926.

[19] Amarouche, M.; Durand, G.; Malrieu, J. P. *J. Chem. Phys.* **1988,** *88,* 1010-1018.

[20] Daskalopoulou, M.; Böhmer, H.-U.; Peyerimhoff, S. D. *Z. Phys. D* **1990,** *15,* 161–169.

[21] Whitaker, B. J.; Woodward, C. A.; Knowles, P. J.; Stace, A. J. *J. Chem. Phys.* **1990,** *93,* 376–383.

[22] Audouard, E.; Spiegelmann, F. *J. Chem. Phys.* **1991,** *94,* 6102–6124.

[23] Ma, N. L.; Li, W.-K.; Ng, C. Y. *J. Chem. Phys.* **1993,** *99,* 3617–3621.

[24] Gadéa, F. X.; Paidarová, I. *Chem. Phys.* **1996,** *209,* 281–290.

[25] Mášik, J.; Urban, J.; Mach, P.; Hubač, I. *Int. J. Quant. Chem.* **1997,** *63,* 333–343.

[26] Naumkin, F. Y.; Wales, D. J. *Mol. Phys.* **1998,** *93,* 633–648.

[27] Heidenreich, A.; Jortner, J. *J. Electron Spectrosc. Relat. Phenom.* **2000,** *106,* 187–197.

[28] Paidarová, I.; Gadéa, F. X. *Chem. Phys.* **2001,** *274,* 1–9.

[29] Ha, T.-K.; Rupper, P.; Wüest, A.; Merkt, F. *Mol. Phys.* **2003,** *101,* 827–838.

[30] Pernpointner, M.; Kryzhvoi, N. V.; Unbaczek, S. *J. Chem. Phys.* **2008,** *129,* 024304.

[31] Ng, C. Y.; Trevor, D. J.; Mahan, B. H.; Lee, Y. T. *J. Chem. Phys.* **1977,** *66,* 446–449.

[32] Dehmer, P. M.; Dehmer, J. L. *J. Chem. Phys.* **1978,** *68,* 3462-3470.

[33] Pratt, S. T.; Dehmer, P. M. *Chem. Phys. Lett.* **1982,** *87,* 533–538.

[34] Dehmer, P. M.; Pratt, S. T.; Dehmer, J. L. *J. Phys. Chem.* **1987,** *91,* 2593–2598.

[35] Tonkyn, R. G.; White, M. G. *J. Chem. Phys.* **1991,** *95,* 5582–5589.

[36] Lu, Y.; Matsui, T.; Tanaka, K.; Ito, K.; Hayaishi, T.; Morioka, Y. *J. Phys. B: At. Mol. Opt. Phys.* **1992,** *25,* 5101–5108.

[37] Pradeep, T.; Niu, B.; Shirley, D. A. *J. Chem. Phys.* **1993,** *98,* 5269–5275.

[38] Hall, R. I.; Lu, Y.; Morioka, Y.; Matsui, T.; Tanaka, T.; Yoshii, H.; Hayaishi, T.; Ito, K. *J. Phys. B: At. Mol. Opt. Phys.* **1995,** *28,* 2435–2451.

[39] Signorell, R.; Wüest, A.; Merkt, F. *J. Chem. Phys.* **1997,** *107,* 10819–10822.

[40] Signorell, R.; Merkt, F. *J. Chem. Phys.* **1998,** *109,* 9762–9771.

[41] Morioka, Y.; Tanaka, T.; Yoshii, H.; Hayaishi, T. *J. Chem. Phys.* **1998,** *109,* 1324–1328.

[42] Onuma, T.; Yoshii, H.; Ishijima, H.; Itou, Y.; Hayaishi, T.; Morioka, Y. *J. Mol. Spectrosc.* **1999,** *198,* 209–217.

[43] Signorell, R.; Hollenstein, U.; Merkt, F. *J. Chem. Phys.* **2001,** *114,* 9840–9851.

[44] Wüest, A.; Rupper, P.; Merkt, F. *Mol. Phys.* **2001,** *99,* 1941–1958.

[45] Rupper, P.; Merkt, F. *J. Chem. Phys.* **2002,** *117,* 4264–4281.

[46] Rupper, P.; Merkt, F. *Mol. Phys.* **2002,** *100,* 3781–3784.

[47] Yoshii, H.; Hayaishi, T.; Onuma, T.; Aoto, T.; Morioka, Y.; Ito, K. *J. Chem. Phys.* **2002,** *117,* 1517–1521.

[48] Fedor, J.; Parajuli, R.; Matt-Leubner, S.; Echt, O.; Hagelberg, F.; Gluch, K.; Stamatovic, A.; Probst, M.; Scheier, P.; Märk, T. D. *Phys. Rev. Lett.* **2003,** *91,* 133401.

[49] Wüest, A.; Merkt, F. *J. Chem. Phys.* **2004,** *120,* 638–646.

[50] Rupper, P.; Zehnder, O.; Merkt, F. *J. Chem. Phys.* **2004,** *121,* 8279–8290.

[51] Yoshii, H.; Tsukamoto, K.; Hayaishi, T.; Aoto, T.; Ito, K.; Morioka, Y. *J. Chem. Phys.* **2005,** *123,* 184303.

[52] Wüest, A.; Merkt, F. *Mol. Phys.* **2005,** *103,* 1285–1300.

[53] Vasilatou, K.; Hollenstein, U.; Merkt, F. *Mol. Phys.* **2010,** *108,* 915–926.

[54] Fedor, J.; Echt, O.; Gluch, K.; Matt-Leubner, S.; Scheier, P.; Märk, T. D. *Chem. Phys. Lett.* **2007,** *437,* 183–188.

[55] Carrington, A.; Gammie, D. I.; Page, J. C.; Shaw, A. M.; Hutson, J. M. *J. Chem. Phys.* **2002,** *116,* 3662–3669.

[56] Zehnder, O.; Mastalerz, R.; Reiher, M.; Merkt, F.; Dressler, R. A. *J. Chem. Phys.* **2008,** *128,* 234306.

[57] Cohen, J. S.; Schneider, B. *J. Chem. Phys.* **1974,** *61,* 3230–3239.

[58] Lefebvre-Brion, H.; Field, R. W. *The Spectra and Dynamics of Diatomic Molecules;* Elsevier: Amsterdam, 2004.

[59] Yamada, C.; Kanamori, H.; Hirota, E. *J. Chem. Phys.* **1985,** *83,* 552–555.

[60] Paul, Th. A.; Liu, J.; Merkt, F. *Phys. Rev. A* **2009,** *79,* 022505.

[61] Tang, K. T.; Toennies, J. P. *J. Chem. Phys.* **2003,** *118,* 4976–4983.

[62] Reiher, M. *Relativistic Douglas-Kroll-Hess theory, in: Wiley Interdisciplinary Reviews: Computational Molecular Science* **2012,** *2,* 139-149.

[63] Roos, B. O.; Lindh, R.; Malmqvist, P.-A. .; Veryazov, V.; Widmark, P.-O. *J. Phys. Chem. A* **2004,** *108,* 2851.

[64] Berning, A.; Schweizer, M.; Werner, H.-J.; Knowles, P. J.; Palmieri, P. *Mol. Phys.* **2000,** *98,* 267.

[65] Werner, H.-J. *et al.* "MOLPRO, version 2002.6, a package of ab initio programs", 2002.

[66] Teachout, R. R.; Pack, R. T. *Atomic Data* **1971,** *3,* 195–214.

[67] Medved', M.; Fowler, P. W.; Hutson, J. M. *Mol. Phys.* **2000,** *98,* 453–463.

[68] Velchev, I.; Hogervorst, W.; Ubachs, W. *J. Phys. B: At. Mol. Opt. Phys.* **1999,** *32,* L511–L516.

[69] Hollenstein, U.; Seiler, R.; Merkt, F. *J. Phys. B: At. Mol. Opt. Phys.* **2003,** *36*, 893–903.

[70] Tanaka, Y.; Yoshino, K.; Freeman, D. E. *J. Chem. Phys.* **1973,** *59*, 5160–5183.

[71] The difference in the zero point energy of the two isotopomers $^{84}Kr_2$ and ^{84}Kr-^{86}Kr amounts to less than $0.01\,cm^{-1}$ and so does the difference in the atomic ionisation energies [69].

[72] Wüest, A.; Merkt, F. *J. Chem. Phys.* **2003,** *118*, 8807–8812.

[73] Wörner, H. J.; Grütter, M.; Vliegen, E.; Merkt, F. *Phys. Rev. A* **2005,** *71*, 052504 see erratum in Phys. Rev. A 73, 059904(E) (2006).

[74] See EPAPS document No. E-JCPSA6-119-X018344 for a table of measured and calculated positions of all vibrational levels of the I(1/2u), I(3/2u), II(1/2u), I(1/2g), I(3/2g) and II(1/2g) states of $^{40}Ar_2^+$ and $^{36}Ar_2^+$ up to 2 cm^{-1} below the corresponding dissociation limits. This document may be retrieved via the EPAPS homepage (http://www.aip.org/pubservs/epaps.html) or from ftp.aip.org in the directory /epaps/. See the EPAPS homepage for more information.

[75] Moore, C. E. *Atomic Energy Levels;* NBS Circular 467/1 National Bureau of Standards: Washington, D. C., 1949.

[76] Moore, C. E. *Atomic Energy Levels;* NBS Circular 467/2 National Bureau of Standards: Washington, D. C., 1952.

[77] Moore, C. E. *Atomic Energy Levels;* NBS Circular 467/3 National Bureau of Standards: Washington, D.C., 1958.

Tables and figures

TABLE I: Spin-orbit interaction matrix in Hund's case (a) basis describing the coupling between the states of $^2\Sigma^+$ and $^2\Pi$ symmetry in the homonuclear rare-gas dimer ions.

	$^2\Sigma^+_{1/2}$	$^2\Pi_{1/2}$	$^2\Pi_{3/2}$
$^2\Sigma^+_{1/2}$	$V_\Sigma(R)$	$-\frac{a(R)}{\sqrt{2}}$	
$^2\Pi_{1/2}$	$-\frac{a(R)}{\sqrt{2}}$	$V_\Pi(R) + \frac{a(R)}{2}$	
$^2\Pi_{3/2}$			$V_\Pi(R) - \frac{a(R)}{2}$

TABLE II: Comparison of the parameters describing $a(R)$ for Ar_2^+, Kr_2^+ and Xe_2^+.

	u states			g states		
	Ar_2^+	Kr_2^+	Xe_2^+	Ar_2^+	Kr_2^+	Xe_2^+
a_0/cm^{-1}	97.5	325.0	597.2	122.9	756.5	1084.5
a_1	1.688	1.636	1.566	0.094	0.230	0.086
a_2	1.632	1.990	2.359	2.902	2.015	2.500

TABLE III: Parameters of the interaction potentials of the lowest electronic states of Ar_2^+. The uncertainties represent 95 % confidence intervals. Parameters given without uncertainties were held fixed.

	u states		g states	
	$^2\Sigma_u^+$	$^2\Pi_u$	$^2\Sigma_g^+$	$^2\Pi_g$
$R_{e,\Lambda}/\text{Å}$	2.41739 ± 0.00037	3.82765 ± 0.00063	5.3967 ± 0.0070	3.0101 ± 0.0024
$D_{e,\Lambda}/\text{cm}^{-1}$	11219.8 ± 1.5	332.633 ± 0.099		1561.83 ± 0.48
β_Λ	1.44268 ± 0.00032	1.4242 ± 0.0016		1.4486 ± 0.0031
$b_\Lambda/\text{Å}^{-1}$	2.75839 ± 0.00038	2.9639 ± 0.0011	2.1709 ± 0.0025	3.1681 ± 0.0029
$C_{4,\Lambda}/(\text{cm}^{-1}\,\text{Å}^4)$ [a,b]	95302	95302	95302	95302
$C_{6,\Lambda}/(\text{cm}^{-1}\,\text{Å}^6)$ [a,b]	511433	243089	511433	243089
A_Λ/cm^{-1} [c]	$1.832 \cdot 10^7$	$1.741 \cdot 10^7$	$5.720 \cdot 10^6$	$3.157 \cdot 10^7$
B_Λ/cm^{-1} [c]	$3.154 \cdot 10^6$	79800		$1.772 \cdot 10^6$
rms	0.84		0.75	
	$a_u(R)$		$a_g(R)$	
a_{Ar^+}/cm^{-1}	954.3887 [a,d]		954.3887 [a,d]	
a_0/cm^{-1}	97.5 [a]		122.9 [a]	
a_1	1.688 [a]		0.094 [a]	
a_2	1.632 [a]		2.902 [a]	

[a]This parameter was kept constant during the fit.
[b]Values from Refs. [66, 67].
[c]Determined from $R_{e,\Lambda}$ and $D_{e,\Lambda}$ using Equations (7) and (8).
[d]Value from Ref. [59].

TABLE IV: Dissociation energies D_e and equilibrium internuclear distances R_e of the lowest six electronic states of Ar_2^+ determined from the potential energy curves displayed in Figs. 4 and 5.

	I(1/2u)	I(3/2g)	I(1/2g) [a]		I(3/2u)	II(1/2u)	II(1/2g)	Reference
			inner	outer well				
D_e/cm^{-1}	10761.8	1568.0	659.2	115.0	330.3	652.4	181.8	This work
	10759	1568	665	113	330	651	177	[49]
	10778	1434	549	79	283	590	134	[29]
	10769	1744	849	-	357	687	66	[24]
$R_e/\text{Å}$	2.418	3.008	3.027	4.871	3.832	3.673	4.517	This work
	2.423	2.996	3.010	4.908	3.805	3.653	4.541	[49]
	2.4047	3.0242	3.0449	5.2745	3.8783	3.6979	4.6865	[29]
	2.410	2.945	2.957	-	3.708	3.606	4.699	[24]

[a]There is a local maximum of the potential energy curve at $R_{\text{max}} = 4.076\,\text{Å}$ and $V(R_{\text{max}}) = E\left(\text{Ar}(^1\text{S}_0) + \text{Ar}^+(^2\text{P}_{3/2})\right) - 75.0\,\text{cm}^{-1}$.

TABLE V: Parameters of the interaction potentials of the lowest *ungerade* electronic states of Kr_2^+. The uncertainties represent 95 % confidence intervals. Parameters given without uncertainties were held fixed.

	$^2\Sigma_u^+$	$^2\Pi_u$
$R_{e,\Lambda}/\text{Å}$	2.68256 ± 0.00022	4.13932 ± 0.00055
$D_{e,\Lambda}/\text{cm}^{-1}$	10922.54 ± 0.52	392.42 ± 0.12
β_Λ	1.37907 ± 0.00028	77.1 [a]
$b_\Lambda/\text{Å}^{-1}$	2.47608 ± 0.00024	3.01931 ± 0.00045
$C_{4,\Lambda}/(\text{cm}^{-1}\,\text{Å}^4)$ [b,c]	144025	144025
$C_{6,\Lambda}/(\text{cm}^{-1}\,\text{Å}^6)$ [b,c]	1028937	498324
A_Λ/cm^{-1} [d]	$2.000 \cdot 10^7$	$5.312 \cdot 10^7$
B_Λ/cm^{-1} [d]	$4.130 \cdot 10^6$	8.440
rms	1.19	
	$a_u(R)$	
$a_{\text{Kr}^+}/\text{cm}^{-1}$	3580.196 [b,e]	
a_0/cm^{-1}	325.0 [b]	
a_1	1.636 [b]	
a_2	1.990 [b]	

[a]This parameter was adjusted by hand. Its large value in combination with the small value of B_Π is a consequence of the weakly bound nature of the $^2\Pi_u$ state.
[b]This parameter was kept constant during the fit.
[c]Values from Ref. [52].
[d]Determined from $R_{e,\Lambda}$ and $D_{e,\Lambda}$ using Equations (7) and (8).
[d]Value from Ref. [60].

TABLE VI: Dissociation energies D_e and equilibrium internuclear distances R_e of the lowest *ungerade* electronic states of Kr_2^+ determined from the potential energy curves displayed in Fig. 7.

	I(1/2u)	I(3/2u)	II(1/2u)	Reference
D_e/cm^{-1}	9361.5	383.0	1099.8	This work
	9360.1	381.9	1091.3	[52]
	9492	260	966	[29]
	9361.2 ± 2.8	382.8 ± 1.9	1099.9 ± 2.1	[43]
$R_e/\text{Å}$	2.692	4.154	3.771	This work
	2.697	4.110	3.732	[52]
	2.6945	4.2132	3.7211	[29]
		4.11 ± 0.04	3.78 ± 0.04	[43]

TABLE VII: Measured positions ($\tilde{\nu}_\mathrm{obs}$) and differences between measured and calculated positions ($\Delta\tilde{\nu} = \tilde{\nu}_\mathrm{calc} - \tilde{\nu}_\mathrm{obs}$) of the vibrational levels of the I(1/2u) state of Ar_2^+. All positions are in cm^{-1} and are given relative to the position of the rovibronic ground state of the corresponding isotopomer of Ar_2^+. The experimental positions include the field-induced shift of the ionisation thresholds. Experimental data from Ref. [74].

| | $^{40}\mathrm{Ar}_2^+$ | | $^{36}\mathrm{Ar}_2^+$ | | | $^{40}\mathrm{Ar}_2^+$ | | $^{36}\mathrm{Ar}_2^+$ | |
v^+	$\tilde{\nu}_\mathrm{obs}$	$\Delta\tilde{\nu}$ [a]	$\tilde{\nu}_\mathrm{obs}$	$\Delta\tilde{\nu}$ [a]	v^+	$\tilde{\nu}_\mathrm{obs}$	$\Delta\tilde{\nu}$ [a]	$\tilde{\nu}_\mathrm{obs}$	$\Delta\tilde{\nu}$ [a]
0		116585.9		116593.3	26	123115.9(30)	−0.5		123391.1
1		116889.5		116913.1	27	123307.9(30)	−1.8		123588.0
2		117188.9		117228.3	28	123496.6(30)	−1.9		123779.9
3	117488.5(30)	4.2		117538.9	29	123681.9(30)	−0.9		123966.8
4		117775.5		117845.0	30	123862.2(30)	−0.5		124148.7
5	118066.1(30)	3.5		118146.4	31	124037.2(30)	−0.9		124325.6
6	118347.8(30)	2.3		118443.2	32	124207.9(30)	−1.0		124497.4
7	118626.3(30)	2.1		118735.3	33	124373.7(30)	−1.6		124664.1
8	118901.4(30)	2.6		119022.8	34	124535.5(30)	−1.5		124825.6
9	119172.3(30)	3.1		119305.7	35	124693.1(6)	−1.0		124981.9
10	119437.4(22)	2.0		119583.9	36	124845.7(7)	−0.9		125133.1
11		119697.5		119857.5	37	124993.9(6)	−0.5		125278.9
12	119955.7(30)	0.4		120126.3	38	125137.1(6)	−0.5	125418.9(7)	−0.6
13	120209.5(30)	0.7		120390.5	39	125275.2(6)	−0.7	125554.4(7)	−0.2
14	120458.8(30)	0.6		120650.0	40	125409.3(7)	−0.2	125684.4(7)	−0.01
15	120703.7(30)	0.4		120904.7	41	125538.6(7)	0.3	125807.8(7)	−0.9
16	120944.5(22)	0.3		121154.7	42	125662.1(6)	−0.1	125927.3(7)	−0.2
17	121180.3(30)	−0.5		121400.0	43	125781.5(7)	0.3	126041.0(7)	0.2
18	121413.2(30)	0.04		121640.5	44	125896.8(7)	1.5	126148.6(7)	0.2
19	121640.5(30)	−0.7		121876.2	45	126004.6(7)	0.3	126250.7(7)	0.3
20	121863.5(30)	−1.5	122106.3(30)	−0.9	46	126108.6(7)	0.2	126347.2(7)	0.6
21	122083.4(21)	−1.0	122332.0(30)	−1.3	47	126207.9(7)	0.6		126437.2
22	122299.2(30)	−0.3		122554.6	48	126301.6(7)	0.4		126522.0
23	122508.6(30)	−1.7		122771.1	49	126391.1(7)	1.2		126601.1
24	122715.5(30)	−1.2		122982.6	50	126474.3(7)	0.9		126674.4
25	122918.0(30)	−0.8		123189.4	DL [b]		127194.282		127193.492

[a]Whenever no experimental data could be determined the calculated values are listed.
[b]DL denotes the position of the $\mathrm{Ar}(^1\mathrm{S}_0) + \mathrm{Ar}^+(^2\mathrm{P}_{3/2})$ dissociation limit.

TABLE VIII: Measured positions ($\tilde{\nu}_{\text{obs}}$) and differences between measured and calculated positions ($\Delta\tilde{\nu} = \tilde{\nu}_{\text{calc}} - \tilde{\nu}_{\text{obs}}$) of the vibrational levels of the I(3/2u) state of Ar_2^+. All positions are in cm^{-1} and are given relative to the position of the rovibronic ground state of the corresponding isotopomer of Ar_2^+. The experimental positions include the field-induced shift of the ionisation thresholds. Experimental data from Ref. [74].

| v^+ | $^{40}\text{Ar}_2^+$ | | $^{36}\text{Ar}_2^+$ | |
	$\tilde{\nu}_{\text{obs}}$	$\Delta\tilde{\nu}$ [a]	$\tilde{\nu}_{\text{obs}}$	$\Delta\tilde{\nu}$ [a]
0	126882.5(15)	−1.2	126882.8(6)	−1.1
1	126919.9(20)	−0.8	126922.8(6)	0.04
2	126954.0(25)	−0.7	126957.9(7)	−0.3
DL [b]		127194.282		127193.492

[a]Whenever no experimental data could be determined the calculated values are listed.
[b]DL denotes the position of the $\text{Ar}(^1\text{S}_0) + \text{Ar}^+(^2\text{P}_{3/2})$ dissociation limit.

TABLE IX: Measured positions ($\tilde{\nu}_{\text{obs}}$) and differences between measured and calculated positions ($\Delta\tilde{\nu} = \tilde{\nu}_{\text{calc}} - \tilde{\nu}_{\text{obs}}$) of the vibrational levels of the II(1/2u) state of Ar_2^+. All positions are in cm^{-1} and are given relative to the position of the rovibronic ground state of the corresponding isotopomer of Ar_2^+. The experimental positions include the field-induced shift of the ionisation thresholds. Experimental data from Ref. [74].

| v^+ | $^{40}\text{Ar}_2^+$ | | $^{36}\text{Ar}_2^+$ | |
	$\tilde{\nu}_{\text{obs}}$	$\Delta\tilde{\nu}$ [a]	$\tilde{\nu}_{\text{obs}}$	$\Delta\tilde{\nu}$ [a]
0	128001.0(7)	−0.8		128002.5
1	128057.0(7)	0.3		128060.3
2	128110.4(7)	1.1		128115.4
DL [b]		128625.865		128625.075

[a]Whenever no experimental data could be determined the calculated values are listed.
[b]DL denotes the position of the $\text{Ar}(^1\text{S}_0) + \text{Ar}^+(^2\text{P}_{1/2})$ dissociation limit.

TABLE X: Measured positions ($\tilde{\nu}_{\mathrm{obs}}$) and differences between measured and calculated positions ($\Delta\tilde{\nu} = \tilde{\nu}_{\mathrm{calc}} - \tilde{\nu}_{\mathrm{obs}}$) of the vibrational levels of the I(1/2g) state of Ar_2^+. All positions are in cm^{-1} and are given relative to the position of the rovibronic ground state of the corresponding isotopomer of Ar_2^+. The experimental positions include the field-induced shift of the ionisation thresholds. Experimental data from Ref. [74].

	$^{40}\mathrm{Ar}_2^+$		$^{36}\mathrm{Ar}_2^+$	
v^+	$\tilde{\nu}_{\mathrm{obs}}$	$\Delta\tilde{\nu}$ [a]	$\tilde{\nu}_{\mathrm{obs}}$	$\Delta\tilde{\nu}$ [a]
0		126589.9 [b]		126592.0 [b]
1	126692.5(30) [b]	-2.5		126702.4 [b]
2	126792.8(15) [b]	-0.8		126805.6 [b]
3	126884.0(15) [b]	-1.1	126899.4(7) [b]	-1.3
4	126968.9(15) [b]	0.3	126986.8(7) [b]	0.1
5	127044.4(20) [b]	2.1		127061.0 [b]
6		127086.8 [b]		127086.4 [b]
7		127100.4 [c]		127101.1 [c]
8		127102.2 [d]		127112.8 [d]
DL [e]		127194.282		127193.492

[a]Whenever no experimental data could be determined the calculated values are listed.

[b]Corresponding vibrational wave function is mostly located in the inner well of the potential energy curve.

[c]Corresponding vibrational wave function is mostly located in the outer well of the potential energy curve.

[d]Corresponding vibrational wave function is located in the inner and the outer well of the potential energy curve.

[e]DL denotes the position of the $\mathrm{Ar}(^1\mathrm{S}_0) + \mathrm{Ar}^+(^2\mathrm{P}_{3/2})$ dissociation limit.

TABLE XI: Measured positions ($\tilde{\nu}_{\mathrm{obs}}$) and differences between measured and calculated positions ($\Delta\tilde{\nu} = \tilde{\nu}_{\mathrm{calc}} - \tilde{\nu}_{\mathrm{obs}}$) of the vibrational levels of the I(3/2g) state of Ar$_2^+$. All positions are in cm^{-1} and are given relative to the position of the rovibronic ground state of the corresponding isotopomer of Ar$_2^+$. The experimental positions include the field-induced shift of the ionisation thresholds. Experimental data from Ref. [74].

| | ^{40}Ar$_2^+$ | | ^{36}Ar$_2^+$ | |
v^+	$\tilde{\nu}_{\mathrm{obs}}$	$\Delta\tilde{\nu}$ [a]	$\tilde{\nu}_{\mathrm{obs}}$	$\Delta\tilde{\nu}$ [a]
0	125685.0(15)	0.2	125687.5(6)	0.4
1	125797.8(20)	−0.3	125806.9(6)	0.6
2	125905.7(15)	−0.9	125920.1(7)	−0.1
3	126009.0(15)	−1.3	126028.9(6)	0.3
4	126107.4(25)	−1.7	126132.0(7)	0.4
5	126202.7(15)	−0.4	126229.6(6)	0.3
6	126292.4(15)	0.1	126321.4(7)	−0.3
7	126376.5(15)	−0.2	126408.9(7)	0.2
8	126455.7(15)	−0.6		126490.4
9	126531.0(30)	−0.1		126566.9
10	126604.0(30)	2.8		126638.1
DL [b]		127194.282		127193.492

[a]Whenever no experimental data could be determined the calculated values are listed.
[b]DL denotes the position of the Ar(^{1}S$_0$) + Ar$^+$(^{2}P$_{3/2}$) dissociation limit.

TABLE XII: Measured positions ($\tilde{\nu}_{\text{obs}}$) and differences between measured and calculated positions ($\Delta\tilde{\nu} = \tilde{\nu}_{\text{calc}} - \tilde{\nu}_{\text{obs}}$) of the vibrational levels of the I(1/2u) state of Kr_2^+. All positions are in cm^{-1} and are given relative to the position of the rovibronic ground state of the corresponding isotopomer of Kr_2^+. The experimental positions include the field-induced shift of the ionisation thresholds. Experimental data from Ref. [52].

	$^{84}\text{Kr}_2^+$		^{84}Kr-$^{86}\text{Kr}^+$			$^{84}\text{Kr}_2^+$		^{84}Kr-$^{86}\text{Kr}^+$	
v^+	$\tilde{\nu}_{\text{obs}}$	$\Delta\tilde{\nu}$ [a]	$\tilde{\nu}_{\text{obs}}$	$\Delta\tilde{\nu}$ [a]	v^+	$\tilde{\nu}_{\text{obs}}$	$\Delta\tilde{\nu}$ [a]	$\tilde{\nu}_{\text{obs}}$	$\Delta\tilde{\nu}$ [a]
0	103773.6(6)	0.5		103772.6	38	109547.5(10)	−2.4		109523.7
1	103956.6(28)	−1.9		103956.9	39	109663.0(15)	−2.2		109638.8
2		104142.2		104139.5	40	109776.1(16)	−2.5		109752.0
3		104324.1		104320.4	41	109888.4(22)	−1.7		109863.3
4		104504.3		104499.6	42	109997.7(20)	−1.8		109972.5
5	104684.4(5)	1.7		104677.0	43	110105.2(19)	−1.8		110079.9
6	104860.6(15)	1.2		104852.7	44	110211.3(23)	−1.2		110185.3
7		105034.2		105026.6	45	110314.2(19)	−1.8		110288.7
8		105207.4		105198.8	46	110416.0(15)	−1.5		110390.1
9		105378.7		105369.3	47	110515.3(23)	−1.6		110489.6
10		105548.3		105537.9	48	110613.4(11)	−1.0		110587.1
11		105716.0		105704.8	49	110708.7(23)	−1.2		110682.6
12		105882.0		105870.0	50	110802.9(25)	−0.5		110776.1
13		106046.2		106033.4	51	110894.2(16)	−0.7		110867.6
14		106208.6		106195.0	52	110983.9(11)	−0.4		110957.1
15	106369.4(7)	0.2		106354.8	53	111071.7(8)	−0.01		111044.6
16	106528.3(12)	0.3		106512.8	54		111157.1		111130.2
17	106685.2(20)	0.3		106669.0	55	111240.8(16)	0.3		111213.7
18	106838.2(28)	−1.9		106823.4	56	111322.7(19)	0.9	111295.7(21)	0.5
19		106993.4		106976.0	57	111401.5(15)	0.4	111375.4(9)	0.6
20	107143.5(17)	−1.3		107126.8	58	111479.7(9)	1.3	111453.6(13)	1.3
21		107294.4		107275.8	59	111555.1(19)	1.4	111529.1(30)	1.3
22	107440.1(20)	−2.1		107422.9	60	111628.9(13)	2.0	111603.2(23)	1.9
23		107588.1		107568.2	61		111698.2		111672.8
24	107730.9(16)	−1.3		107711.7	62	111769.2(15)	1.8		111742.4
25	107872.8(22)	−1.6		107853.3	63	111837.2(19)	2.7		111809.9
26	108012.8(12)	−1.9		107993.1	64	111902.2(14)	2.5		111875.4
27	108150.7(26)	−2.4		108131.0	65	111965.6(13)	2.8		111938.9
28	108288.3(10)	−1.3		108267.1	66	112027.0(12)	3.0		112000.5
29	108422.7(16)	−1.6		108401.3	67	112086.8(29)	3.7		112060.0
30		108557.0		108533.6	68		112140.2		112117.6
31		108687.9		108664.0	69	112199.0(11)	3.6		112173.2
32	108814.7(12)	−2.1		108792.5	70		112248.5		112226.9
33	108942.5(17)	−1.3		108919.2	71		112299.7		112278.6
34		109068.9		109043.9	72		112348.9		112328.3
35	109190.0(14)	−2.1		109166.7	73	112399.8(15)	3.7		112376.1
36	109310.9(13)	−2.4		109287.6	74	112445.5(11)	4.1		112422.0
37	109430.0(16)	−2.6		109406.6	DL [b]		113041.23		113041.23

[a]Whenever no experimental data could be determined the calculated values are listed.
[b]DL denotes the position of the Kr($^1S_0$) + Kr$^+$($^2P_{3/2}$) dissociation limit.

TABLE XIII: Measured positions ($\tilde{\nu}_{\mathrm{obs}}$) and differences between measured and calculated positions ($\Delta\tilde{\nu} = \tilde{\nu}_{\mathrm{calc}} - \tilde{\nu}_{\mathrm{obs}}$) of the vibrational levels of the I(3/2u) state of Kr_2^+. All positions are in cm^{-1} and are given relative to the position of the rovibronic ground state of the corresponding isotopomer of Kr_2^+. The experimental positions include the field-induced shift of the ionisation thresholds. Experimental data from Ref. [52].

| | $^{84}\mathrm{Kr}_2^+$ | | $^{84}\mathrm{Kr}$-$^{86}\mathrm{Kr}^+$ | |
v^+	$\tilde{\nu}_{\mathrm{obs}}$	$\Delta\tilde{\nu}$ [a]	$\tilde{\nu}_{\mathrm{obs}}$	$\Delta\tilde{\nu}$
0	112672.4(2)	0.08	112672.4(4)	0.2
1	112699.6(3)	0.2	112699.4(6)	0.2
2	112725.0(3)	−0.2	112724.9(6)	0.1
3	112749.4(3)	0.08	112748.9(7)	−0.1
4	112772.2(4)	−0.3	112771.6(5)	−0.3
5	112793.8(3)	−0.3	112793.3(10)	−0.1
6	112814.3(7)	−0.2	112813.1(14)	−0.6
7	112833.2(9)	−0.4		112832.8
8	112851.2(4)	−0.3		112850.6
9	112867.8(7)	−0.4		112867.3
10	112883.1(7)	−0.7		112882.9
DL[b]		113041.23		113041.23

[a]Whenever no experimental data could be determined the calculated values are listed.
[b]DL denotes the position of the $\mathrm{Kr}(^1\mathrm{S}_0) + \mathrm{Kr}^+(^2\mathrm{P}_{3/2})$ dissociation limit.

TABLE XIV: Measured positions ($\tilde{\nu}_{obs}$) and differences between measured and calculated positions ($\Delta\tilde{\nu} = \tilde{\nu}_{calc} - \tilde{\nu}_{obs}$) of the vibrational levels of the $\Pi(1/2u)$ state of Kr_2^+. All positions are in cm^{-1} and are given relative to the position of the rovibronic ground state of the corresponding isotopomer of Kr_2^+. The experimental positions include the field-induced shift of the ionisation thresholds. Experimental data from Ref. [52].

| v^+ | $^{84}Kr_2^+$ | | ^{84}Kr-$^{86}Kr^+$ | |
	$\tilde{\nu}_{obs}$	$\Delta\tilde{\nu}$ [a]	$\tilde{\nu}_{obs}$	$\Delta\tilde{\nu}$
0	117339.3(10)	−0.3		117339.5
1	117394.3(11)	−0.1		117393.9
2	117447.6(4)	−0.06		117446.9
3	117499.5(5)	0.09	117498.4(10)	0.03
4	117549.8(4)	0.1	117548.4(7)	0.05
5	117598.7(5)	0.3	117597.0(6)	0.2
6	117645.8(5)	0.2	117644.2(9)	0.4
7	117691.9(7)	0.7	117689.9(12)	0.7
8	117736.1(13)	0.8	117734.1(12)	0.9
9		117777.9	117776.8(22)	1.2
DL [b]		118411.53		118411.53

[a]Whenever no experimental data could be determined the calculated values are listed.
[b]DL denotes the position of the $Kr(^1S_0) + Kr^+(^2P_{1/2})$ dissociation limit.

FIG. 1: The spin-orbit coupling constant $a(R)$ in Ar_2^+, Kr_2^+ (this work) and Xe_2^+ (from Ref. [56]) obtained from Davidson-corrected DKH2 MRCISD calculations. The horizontal lines at large distances mark the position of asymptotic value of the spin-orbit-coupling constants determined by atomic spectroscopy which have been taken from Refs. [59, 75] (Ar^+), [60, 76] (Kr^+) and [77] (Xe^+)
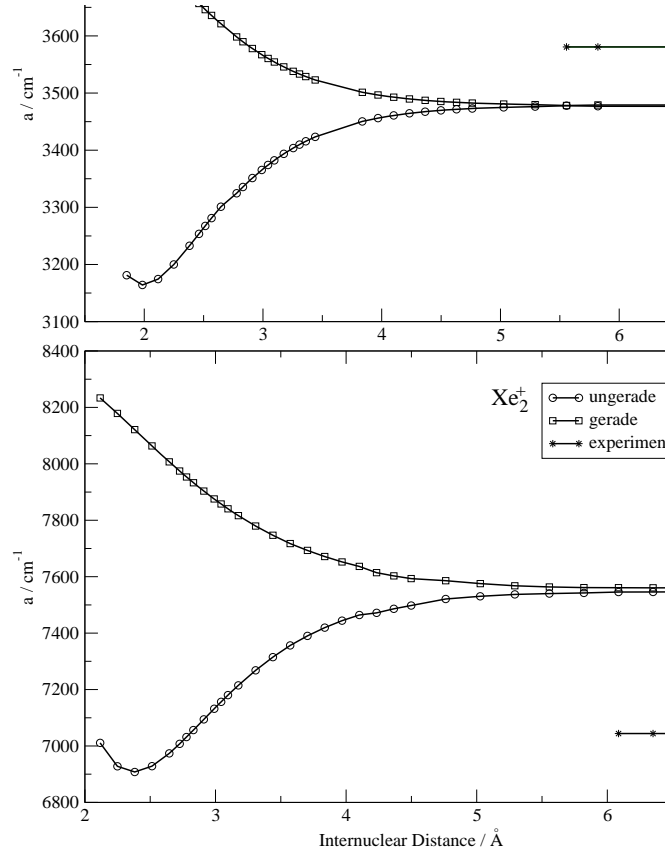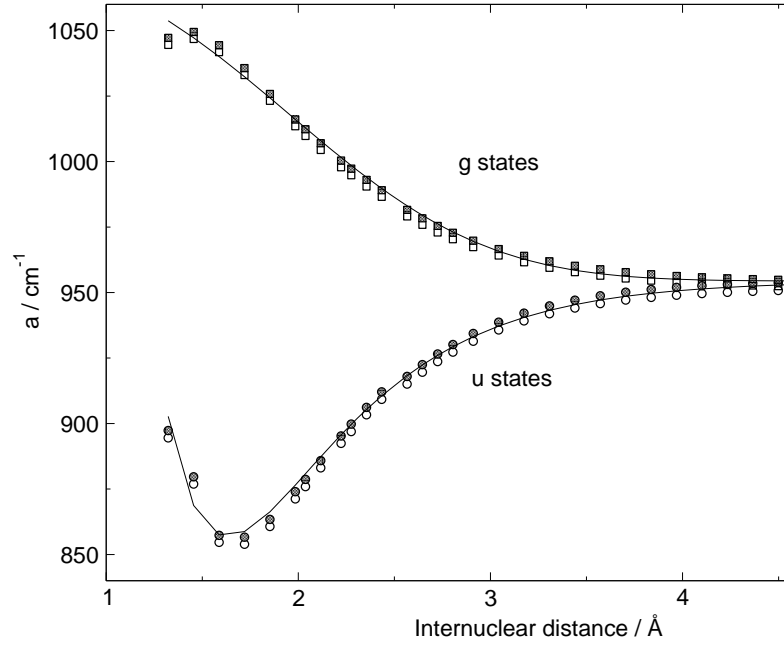
FIG. 2: R-dependent spin-orbit-coupling constant $a(R)$ for the u (circles) and the g (squares) states of Ar_2^+ derived from DKH2 MRCI+Q *ab initio* calculations (open circles and squares). The filled circles and squares are scaled such that the asymptotic value is equal to the spin-orbit splitting of the Ar^+ ^2P ground state. The full lines represent fits based on the expressions in Eqs. (5) and (6).
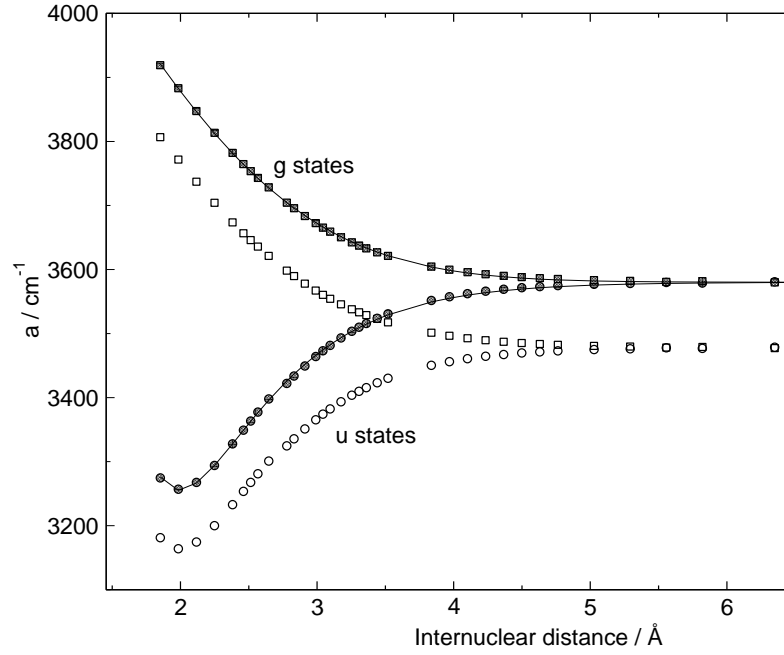
FIG. 3: R-dependent spin-orbit-coupling constant $a(R)$ for the u (circles) and the g (squares) states of Kr_2^+ derived from DKH2 MRCI+Q *ab initio* calculations (open circles and squares). The filled circles and squares are scaled such that the asymptotic value is equal to the spin-orbit splitting of the Kr^+ ${}^2P$ ground state. The full lines represent fits based on the expressions in Eqs. (5) and (6).
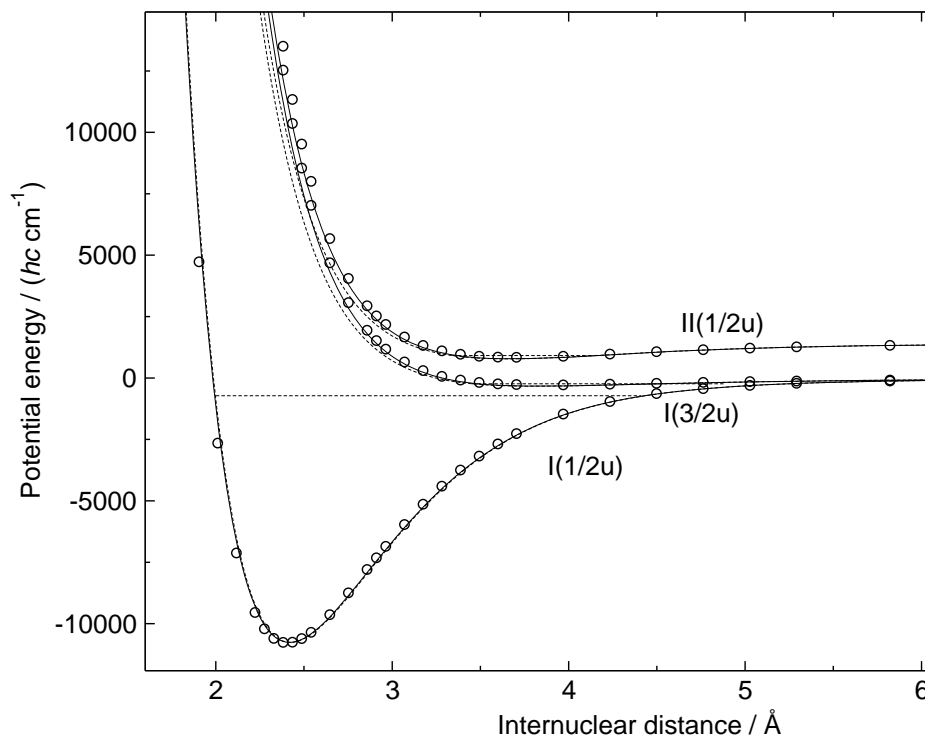
FIG. 4: Comparison of the potential energy functions of the I(1/2u), I(3/2u) and II(1/2u) states of Ar_2^+ derived in this work (full line), in Ref. [49] (dashed line) and in Ref. [29] (circles). The dashed horizontal lines indicate for each state the positions of the highest observed vibrational level.
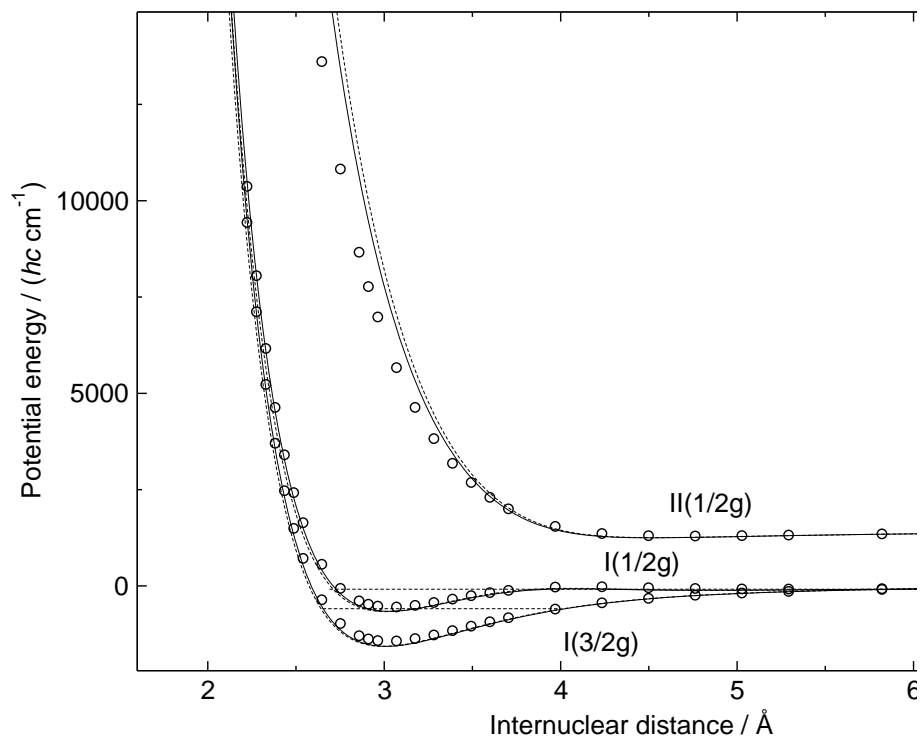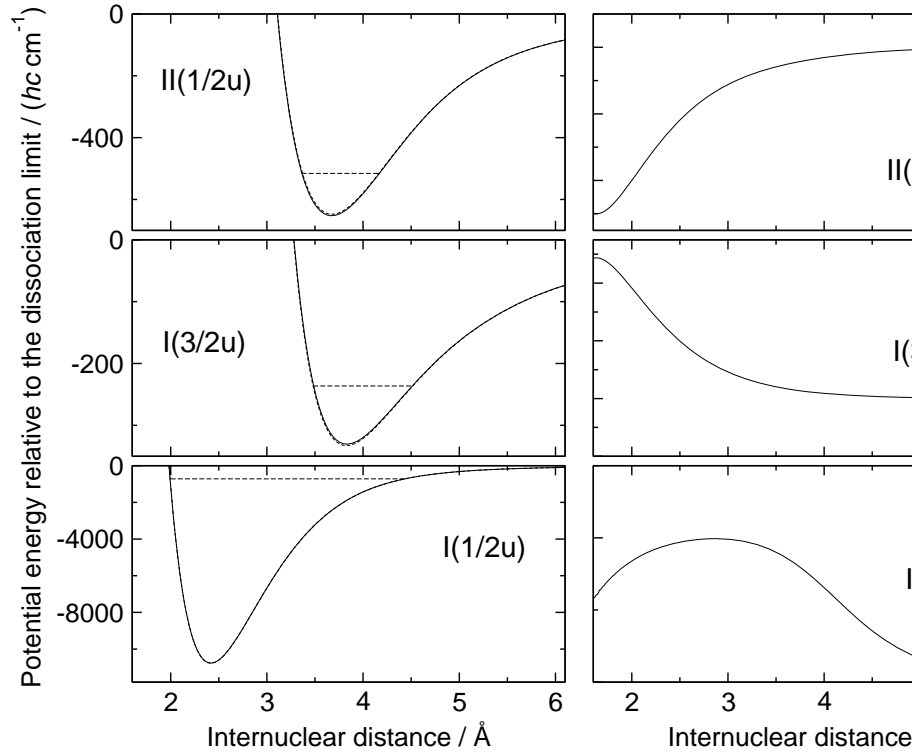
FIG. 5: Comparison of the potential energy functions of the I($3/2g$), I($1/2g$) and II($1/2g$) states of Ar_2^+ derived in this work (full line), in Ref. [49] (dashed line) and in Ref. [29] (circles). The dashed horizontal lines indicate for each state the positions of the highest observed vibrational level.

FIG. 6: Left panels: Potential energy functions of the I(1/2u) (bottom), I(3/2u) (middle) and II(1/2u) (top) states of Ar_2^+ calculated with R-dependent $a_u(R)$ (full lines) and R-independent $a = a_{Ar^+}$ (dashed lines) using the same Σ and Π potential energy curves (parameter set for the u states in Table III). The dashed horizontal lines indicate for each state the positions of the highest observed vibrational level. Right panels: Energy difference of the two curves displayed in the left panels for the I(1/2u) (bottom), I(3/2u) (middle) and II(1/2u) (top) states of Ar_2^+.
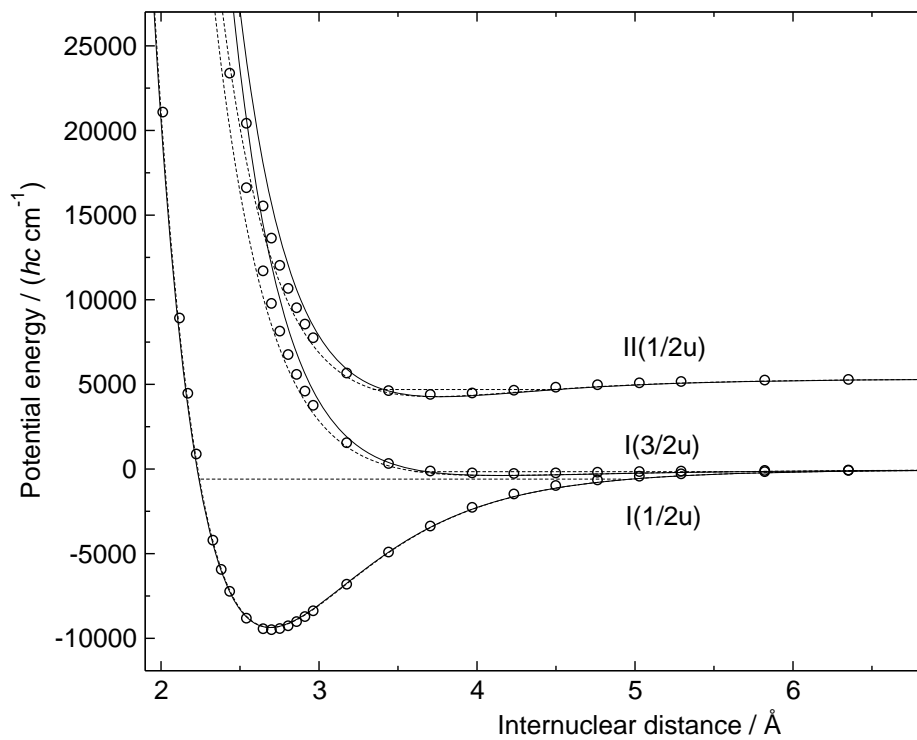
FIG. 7: Comparison of the potential energy functions of the I(1/2u), I(3/2u) and II(1/2u) states of Kr_2^+ derived in this work (full line), in Ref. [52] (dashed line) and in Ref. [29] (circles). The dashed horizontal lines indicate for each state the positions of the highest observed vibrational level.
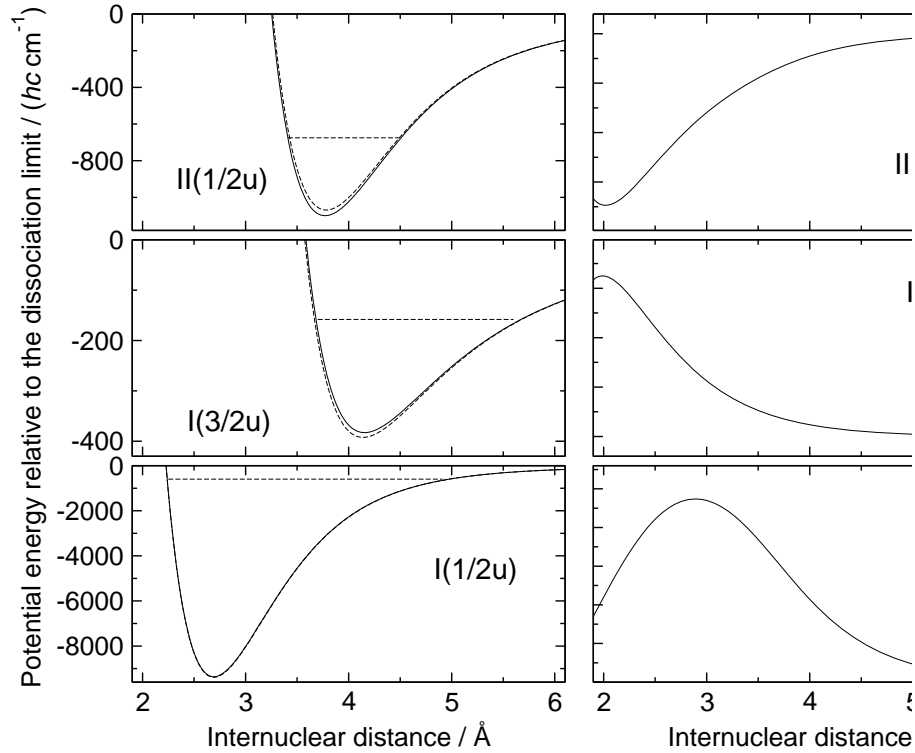
FIG. 8: Left panels: Potential energy functions of the I($1/2u$) (bottom,), I($3/2u$) (middle) and II($1/2u$) (top) states of Kr_2^+ calculated with R-dependent $a_u(R)$ (full lines) and R-independent $a = a_{Kr^+}$ (dashed lines) using the same Σ and Π potential energy curves (parameter set for the u states in Table V). The dashed horizontal lines indicate for each state the positions of the highest observed vibrational level. Right panels: Energy difference of the two curves displayed in the left panels for the I($1/2u$) (bottom), I($3/2u$) (middle) and II($1/2u$) (top) states of Kr_2^+.